Int. J. Electrochem. Sci., 7 **(2012)** 6638 - 6653

International Journal of
ELECTROCHEMICAL
SCIENCE
www.electrochemsci.org

Surface Coloration and Electrochemical Impedance Spectroscopy Characterization of Oxygen Plasma Implanted Orthopaedic Titanium Alloys

Xiangmei Liu[1], *Shuilin Wu*[1, 2,*], *Kelvin W. K. Yeung*[3], *C.Y. Chung*[2], *Paul K Chu*[2,*]

[1] Ministry-of-Education Key Laboratory for the Green Preparation and Application of Functional Materials, School of Materials Science and Engineering, Hubei University, Wuhan, Peoples' Republic of China, 430062
[2] Department of Physics & Materials Science, City University of Hong Kong, Tat Chee Avenue, Kowloon, Hong Kong, China
[3] Division of Spine Surgery, Department of Orthopaedics and Traumatology, The University of Hong Kong, Pokfulam, Hong Kong, China
[*]E-mail: paul.chu@cityu.edu.hk; shuilin.wu@gmail.com

Received: 3 July 2012 / *Accepted:* 19 July 2012 / *Published:* 1 August 2012

Oxygen plasma immersion ion implantation (O-PIII) is performed at different frequencies to produce stable passive films with different color on titanium alloys. UV-visible reflectance spectra acquired from these films show that the strong reflection region shifts to long wavelength as the implantation frequency or time is increased. X-ray photoelectron spectroscopy indicates that these passive films possess three layers with different thicknesses and chemical compositions. As the frequency is increased, both the outer and intermediate layers become thicker while the thickness of gradient transition layer changes only slightly. EIS spectra and simulated results reveal that the implantation frequency and duration significantly influence the structure, chemical composition, and color of these passive films.

Keywords: Coloration; Titanium Alloy; Passive Film; Plasma Immersion Ion Implantation; EIS

1. INTRODUCTION

Passive layers with different color can be produced on titanium-based alloys by different techniques such as heat treatment at high temperature, anodization, laser irradiation, chemical reaction, and reactive magnetron sputtering [1-6]. Besides better chemical stability, the good wear resistance and corrosion resistance rendered by these passive films act as natural barriers for the titanium substrates in the complex biological environment to reduce wear debris and ion leaching consequently

improving the cytocompatibility and favoring long-term fixation of orthopedic titanium implants [7-12]. In addition, they can serve as intermediates for further biomimetic treatment on the surface in order to achieve better biological activities [12-15]. Therefore, formation of stable titanium oxide films on the surface is critical to clinical applications of titanium-based alloys as orthopedic implants.

Although the aforementioned methods can produce colored titanium oxide films, there are some shortcomings. For instance, during thermal oxidation, the high temperature can impair the mechanical property, and undesired ions like Cl^- or F^- may be introduced into the surface layer during electrochemical anodization [3]. Addition of hydrogen peroxide to the phosphate buffer solution (PBS) can increase the formation rate of the blue titanium oxide film but a discontinuous outer layer forms easily during this process and other elements are usually incorporated into this porous layer [16]. As a non-line-of-sight surface modification technique, oxygen plasma immersion ion implantation (O-PIII) is an effective method to prepare protective metallic oxides films on biomedical metals despite the complex surface topography [17-19]. Our previous studies focused on the effects of the surface titanium oxide layers formed by O-PIII on the biocompatibility, tribological behavior, as well as corrosion resistance [11, 20-23], but to the best of our knowledge, there have been no studies on the relationship between surface coloration and characteristics of passive layers produced by O-PIII on titanium alloys. In this work, the effects of the passive layer produced by O-PIII on orthopedic Ti6Al4V alloy using different parameters on surface coloration are investigated systematically.

2. EXPERIMENTAL PROCEDURES

Titanium alloy (Ti-6Al-4V) bars with 4% vanadium, 6% aluminum, and less than 0.2% iron and oxygen (Goodfellow) were cut into 1 mm thick disks with a diameter of 5 mm. They were mechanically ground by SiC sandpaper progressively up to 2400 grit, ultrasonically rinsed with acetone and ethanol, and oven-dried before further experiments. After the samples were sputtered with argon plasma at 5 kV to remove surface contaminants, O-PIII was carried out in the plasma immersion ion implanter at City University of Hong Kong [22].

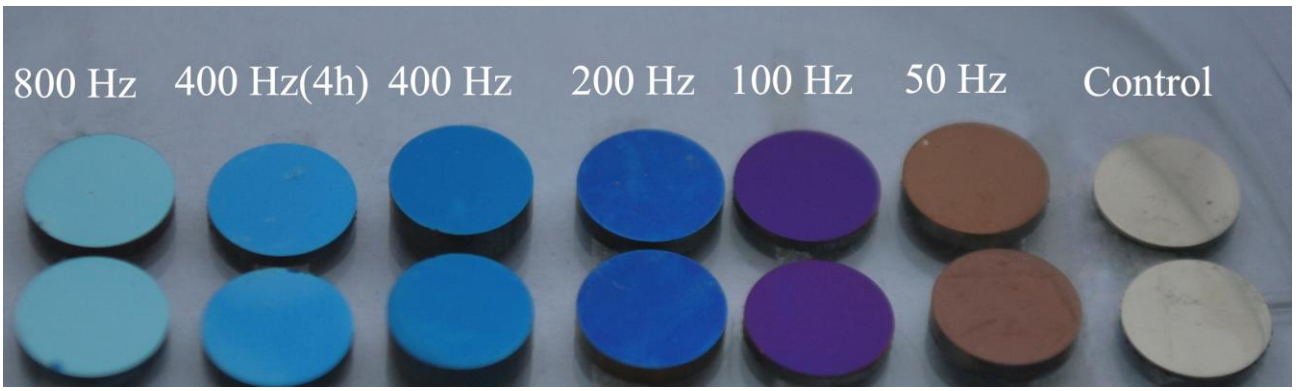

Figure 1. Color variation on the various Ti6Al4V samples prepared by O-PIII.

The main instrumental parameters were: implantation power (RF) = 1 kW; working pressure = 3.4 x 10^{-4} Torr; implantation voltage = -40 kV, and pulse width = 100 μs. Five implantation frequencies of 50 Hz, 100 Hz, 200 Hz, 400 Hz, and 800 Hz were selected together with an implantation time of 2 hrs. For comparison, another batch of samples was implanted at 400 Hz for 4 hrs. The mechanically polished sample labeled as MP was the control. After O-PIII, the samples exhibited different colors as shown in Fig. 1.

The chemical composition of passive films was determined by high-resolution X-ray photoelectron spectroscopy (XPS; Physical Electronics PHI 5802, Minnesota, MN). The take-off angle was 45^o and base vacuum was 2 x 10^{-8} Pa. Survey scans spanning a binding energy range of 0 to 1200 eV at a pass energy of 187.85 eV and 0.8 eV per step were first acquired to identify the elemental species. High-resolution scans were subsequently acquired at a pass energy of 11.75 eV and 0.1 eV per step. A Gaussian-Lorentzian peak-fitting model was used to deconvolute the spectra. In the depth profiling analysis, the sputtering rate was about 9.75 nm/min and the profiles were terminated when the atomic concentrations of the detected elements reached equilibrium values. The evolution of Ti 2p with depth was monitored by high-resolution XPS.

The light reflecting properties of the passive layers produced by O-PIII on the titanium alloy samples were determined by acquiring the UV–visible reflective spectra on the Perkin Elmer Lambda 750 in the wavelength range of 300 – 800 nm. The electrochemical behavior of the untreated and O-PIII titanium alloys were characterized in simulated body fluid solution (SBF) at 37±0.5^{o}C and pH of 7.42. The SBF was composed of 7.996 g/l of NaCl, 0.35 g/l of $NaHCO_3$. 0.224 g/l of KCl, 0.228 g/l of $K_2HPO_4{\cdot}3H_2O$, 0.305 g/l of $MgCl_2{\cdot}6H_2O$, 0.278 g/l of $CaCl_2$, 0.071 g/l of Na_2SO_4, as well as 6.057 g/l $(CH_2OH)_3CNH_2$ and the ion concentrations mimic those in the human blood plasma [24]. A standard three-electrode apparatus was placed in a glass cell immersed in a 37±0.5^{o}C water bath filled with SBF with the working electrodes being the titanium alloy plates. The working electrodes with an exposed area of 0.196 cm^2 were sealed with epoxy powders using a hot mounting press (Buehler, USA) at 150 ^{o}C to prevent the electrolyte from permeating. The counter electrodes consisted of two graphite rods mounted diametrically opposite to each other and the reference electrode was a saturated calomel electrode (SCE). Electrochemical impedance spectroscopy (EIS) was carried out at open-circuit potentials (OCP) using an EG&G PAR Model 273A potentiostat / galvanostat and a PAR Model 5210 lock-in-amplifier. The system was controlled by a personal computer equipped with the PAR Model 398 software. A sinusoidal AC (alternating current) voltage of ±5 mV was applied during the impedance measurements and the impedance response was determined in the frequency range from 5 mHz to 100 kHz. The EIS analysis software ZSimpWin (Version 3.21) was used to model the impedance data and extract the resistance and capacitance data. This software utilized the "downhill simplex method" based on a trial-and-error method to find the best fit for the given set of data and a chosen equivalent electrical circuit (EEC). The parameters including the chi-square values and the error distributions were used as weight-factors to provide the closest fits to the model. In order to minimize statistical errors, the EIS measurements were conducted 3 times on samples in the same lot under the same conditions.

3. RESULTS AND DISCUSSION

As shown in Fig. 1, the titanium alloys after O-PIII at different implantation frequencies from 50 to 800 Hz show different colors. The mechanically polished (MP) titanium alloy displays a shiny metallic color and as the implantation frequency is increased, the alloys exhibit different colors varying from bluish purple to different shades of blue and light green. The sample implanted at 400 Hz for 4 hours is not as blue as that treated for 2 hours. The colored surface layers produced by O-PIII are very stable and do not discolor in air or in simulated physiological environments. It is generally accepted that light interference between the interfaces is responsible for the observed color of the passive layer on a metal surface [25]. For example, Van Gils, et al.'s study revealed that reflection from the passive layer determined the color saturation and appearance of the metal [26].

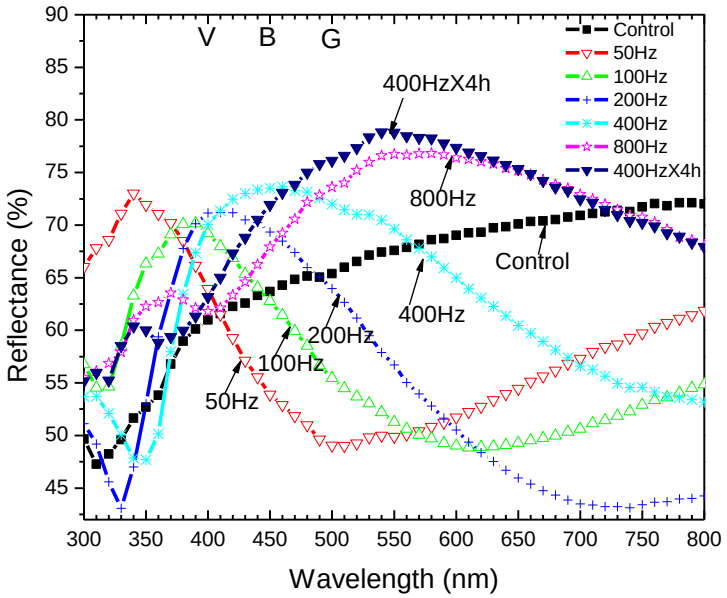

Figure 2. UV-vis reflectance spectra of the MP and O-PIII titanium alloys.

The UV-vis reflectance spectra are displayed in Fig. 2. The reflectance values oscillate between 43% and 78%, and the maximum is observed from the 400 Hz - 4 h sample, followed by 800 Hz - 2 h sample. Generally, as the frequencies diminish, there are more fluctuations in the reflectance in the spectrum. The MP sample does not show an obvious maximum reflective wavelength and there is high reflection throughout the entire visible wavelengths. Hence, the control sample has the silver appearance of a typical metal. The maximum reflectance values from the O-PIII titanium alloys treated at 50, 100, 200, 400, and 800 Hz for 2 hours are at 341, 385, 402, 453, 540 nm, respectively, showing that an increased frequency leads to a redshift. Prolonging the implantation produces a similar effect. For example, as shown in Fig.2, the maximum absorption peak is at 545 nm after implantation for 4 hours at 400 Hz. It is also obvious that the absorption peak becomes wider as the implantation frequencies go up. Although the stronger reflectance of 50 Hz samples falls in the ultraviolet region, the reflection value in the near violet light region is higher than that in visible light

region. Therefore, these samples display a violet color. As the implantation frequency is further increased, the strong reflection regions for the samples treated at 100, 200, 400 Hz shift to the blue wavelengths and consequently those samples show two-tone blue colors. Because the UV-vis reflectance spectra acquired from both the 400 Hz - 4 h and 800 Hz - 2 h samples show stronger reflection in the green wavelength range, they appear green. The UV-vis reflectance spectra show that the properties of the passive layers can influence the surface characteristics significantly, five types of samples (MP, 50 Hz for 2 hours, 200 Hz for 2 hours, 800 Hz for 2 hours and 400 Hz for 4 hours) are selected for further studies by XPS and EIS.

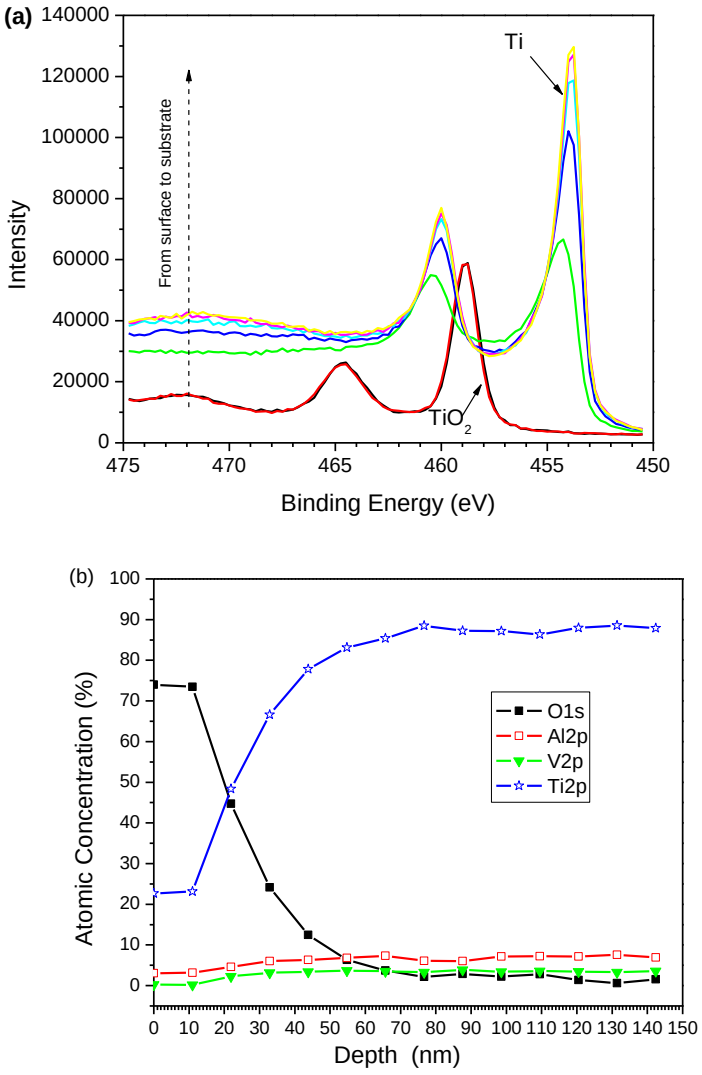

Figure 3. XPS analysis of the mechanically polished titanium alloy: (a) High resolution narrow scan of Ti 2p and (b) Depth profile.

Fig. 3a depicts the high-resolution narrow scan of the typical Ti2p peak of the untreated Ti alloy. The binding energy of $Ti2p_{3/2}$ peak in the top layer is 458.8 eV whereas the second value is about 453.8 eV, corresponding to quad-valence titanium and metallic titanium [27, 28], respectively.

Hence, on the untreated titanium, the outer layer is composed of TiO_2 and followed by almost metallic titanium underneath without an intermediate layer. The depth profile in Fig. 3b reveals that the thickness of this outer layer is about 10 nm.

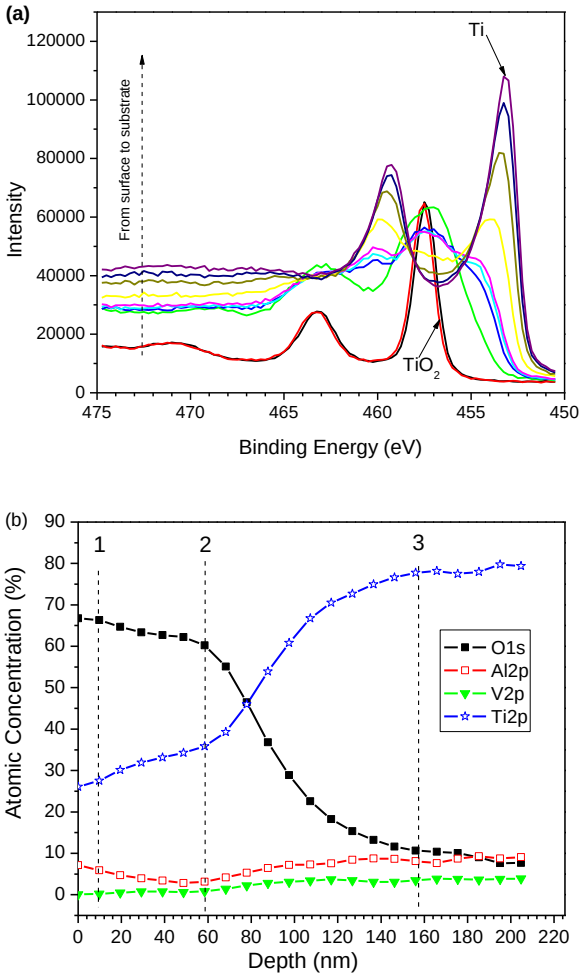

Figure 4. XPS analysis of the titanium alloy treated by O-PIII at 50 Hz for 2 h: (a) High-resolution narrow scan of Ti 2p and (b) Depth profile.

The high-resolution XPS spectra of the 50Hz O-PIII sample is shown in Fig. 4a. According to the variation of the binding energy of $Ti2p_{3/2}$ with depth, the outer layer is composed of titanium dioxide similar to the MP sample. However, there is a series of superpositioned peaks of $Ti2p_{3/2}$ between metallic titanium and quad-valence titanium. According to the reported fitted results of the intermediate peaks, the main constituents are TiO_2, Ti_2O_3, TiO, and Ti in this transition layer [29, 30]. At larger depths, the TiO_2 content diminishes while metallic Ti becomes more dominant gradually. The depth profile in Fig.4b reveals a stable TiO_2 film of about 59 nm followed by a 100 nm transition layer. With regard to the 200 Hz or 800 Hz O-PIII samples, as shown in Figs 5a and 6a, the high-resolution XPS narrow scan spectra of Ti2p exhibit similar characteristics, i.e. an outer TiO_2 layer, a gradient transition layer composed of TiO_2, Ti_2O_3, TiO and Ti, and then the substrate.

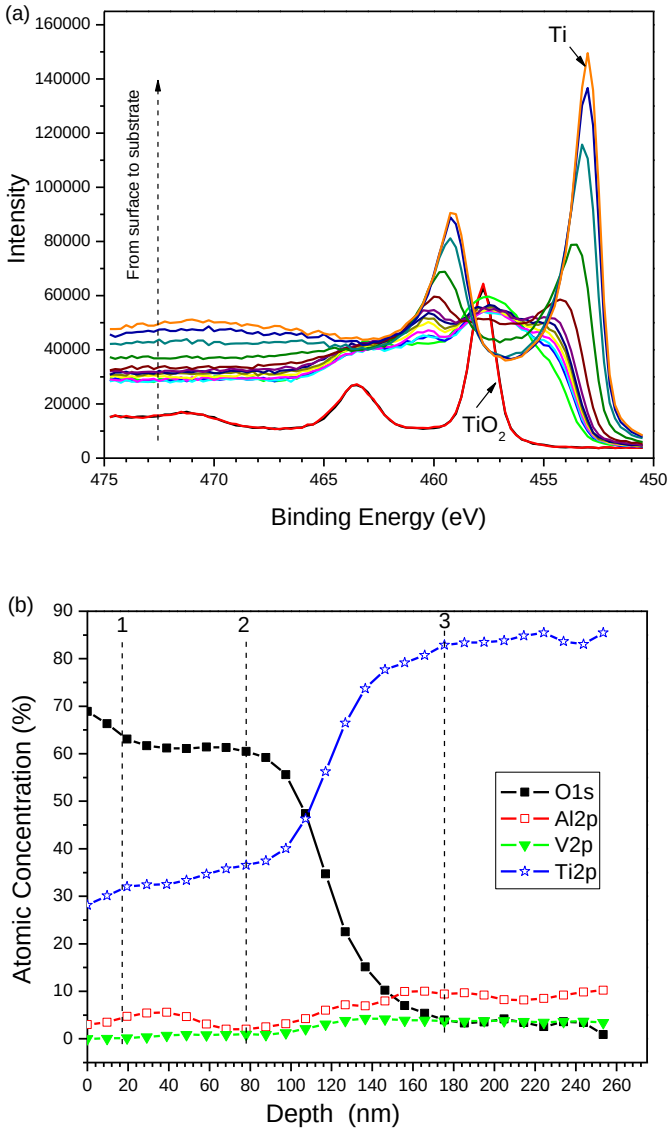

Figure 5. XPS analysis of the titanium alloy treated by O-PIII at 200 Hz for 2 h: (a) High-resolution narrow scan of Ti 2p and (b) Depth profile

The thicknesses of these layers shown in the depth profiles in Figs. 5b and 6b are different. The thickness of the stable TiO_2 layer in the former (200 Hz) is near 80 nm whereas that of the latter (800Hz) is about 150 nm. The results suggest that a larger implantation frequency increases the thickness of the TiO_2 layer. As shown in Fig. 7, the high-resolution XPS spectra and depth profile of the O-PIII sample (400 Hz for 4 h) show results similar to those of the 800 Hz – 2 h sample (Fig. 6), indicating that a longer implantation duration can produce a similar passive film. However, the thickness of the transition layer shows no apparent difference among the O-PIII samples.

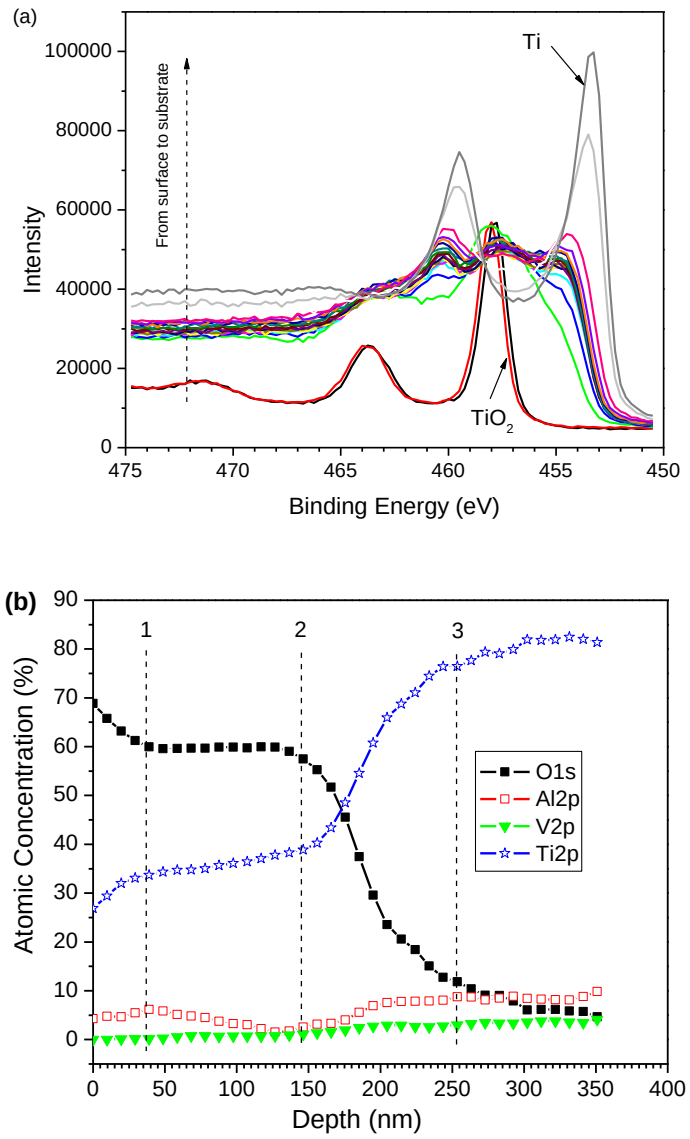

Figure 6. XPS analysis of the titanium alloy treated by O-PIII at 800 Hz for 2 h: (a) High-resolution narrow scan of Ti 2p and (b) Depth profile

As an effective technique for interfacial analysis, electrochemical impedance spectroscopy (EIS) is usually used to characterize the passive films formed on pure metals or alloys. Pan, et al. proposed a bilayer structure of oxide films on titanium composed of a porous outer layer and dense inner layer of TiO_2, and they also modeled the experimental results by EIS using corresponding equivalent electrical circuits (EEC) [31]. This model was confirmed by other researchers and successfully used to explain the surface and interfacial behaviors of passive layers formed on titanium-based alloys in a mimicking biological environment [32-38]. Here, on the basis of our XPS analysis, the physical model of the mechanically polished (MP) titanium alloys is illustrated in Fig. 8a. The passive layer on MP comprises a dominant porous TiO_2 outer layer 10 nm thick and then a thin transition layer. The relevant EEC1 diagram is shown in Fig. 8b, where *Rs* is the resistance of the electrolyte SBF, *Ro* and *Rt* represent the additional resistance of the electrolyte inside the outer porous

structure and charge transfer resistance of the transition layer [32, 35, 38], respectively, *Ct* stands for the interfacial capacitance of the transition layer beneath porous TiO_2 layer, *Qo* is the constant phase element (CPE) of the entire oxide layer.

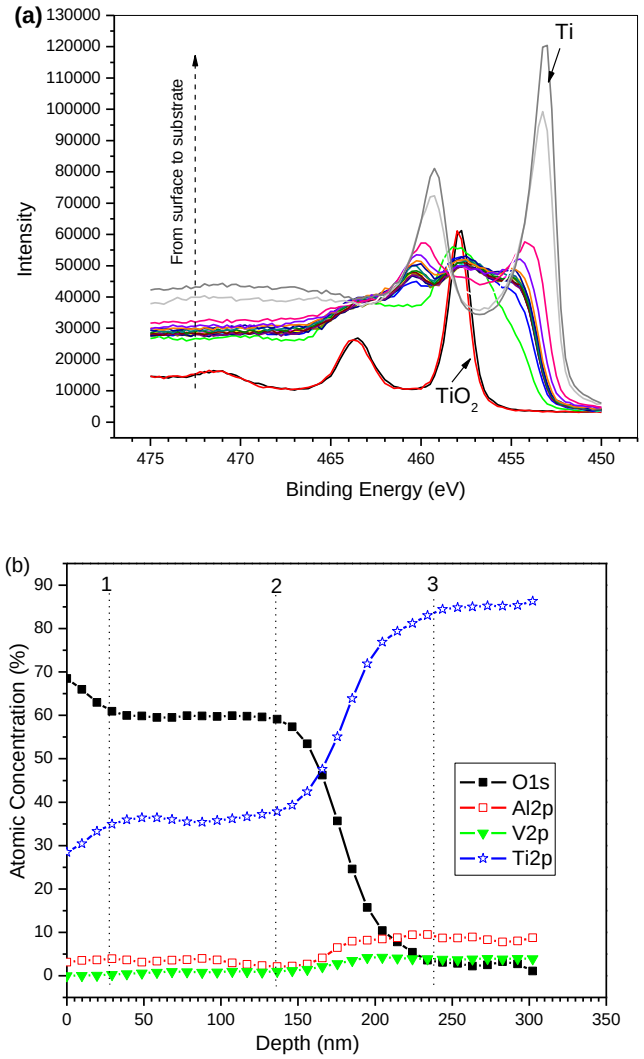

Figure 7. XPS analysis of the titanium alloy treated by O-PIII at 400 Hz for 4 h: (a) High-resolution narrow scan of Ti 2p and (b) Depth profile

CPE is used to describe the deviation from the ideal capacitor behavior and the impedance of a CPE is defined as $Z_{CPE} = [Q\ (jw)^{n}]^{-1}$, where Q is the CPE constant, n is the CPE exponential factor ($-1 \leq n \leq 1$) which is related to the electrode roughness and heterogeneity, j is the imaginary number, ω is the angular frequency, and (jw) presents the complex variable for sinusoidal perturbations [39-41]. In the ideal case when n = 1, CPE acts as a pure capacitor and Q is equal to the capacitance C. The EIS results acquired from the MP titanium alloy immersed in SBF at 37 ^{o}C are presented by the Bode diagrams. As shown in Fig. 9, at the frequency range higher than 10^4 Hz, the impedance ($\mathrm{Log}|Z|$) is almost constant as a function of frequency ($\mathrm{Log}|f|$). This phenomenon is caused by a typical resistive behavior, corresponding to the resistance of the solution between the reference and working electrode.

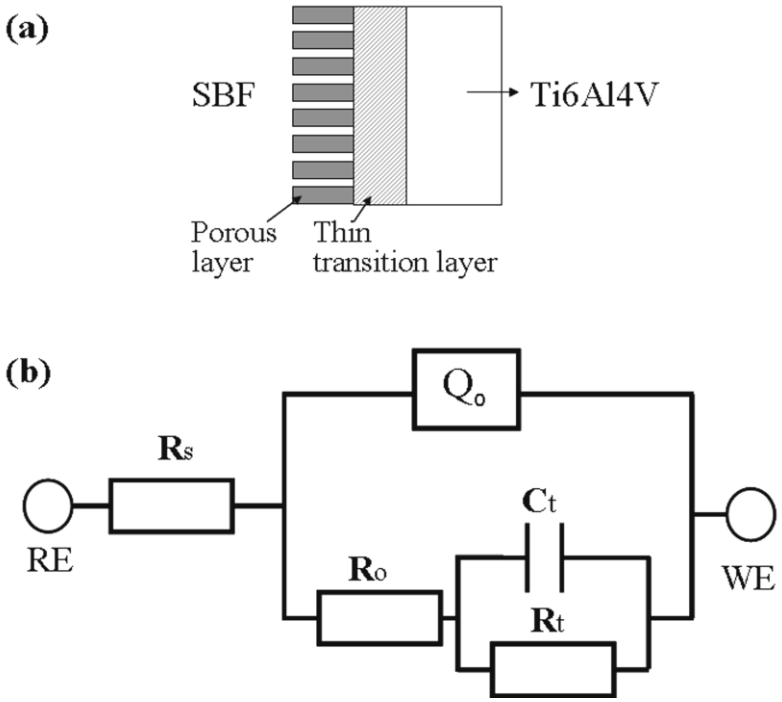

Figure 8. (a) Physical model of the interface between SBF and mechanically polished Ti6Al4V alloys at open circuit potentials and (b) Equivalent electrical circuit 1 (EEC1)

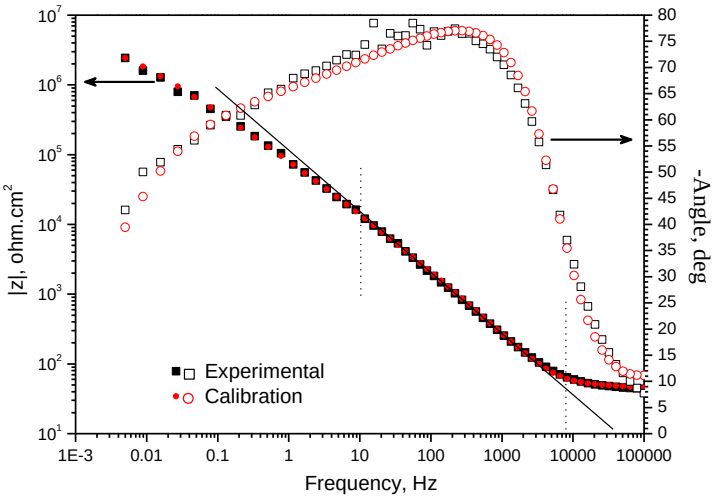

Figure 9. Bode diagrams of the mechanically polished Ti6Al4V (control sample) in SBF at 37 ^{o}C and EIS is modeled by EC1.

The similar phenomenon is observed from the EIS spectra of all the O-PIII samples shown in Fig. 11. In the medium frequency range between about 10 Hz and 10^4 Hz, there is a large negative phase angle approaching nearly -80^{o} and the impedance ($\mathrm{Log}|Z|$) increases linearly as the frequency ($\mathrm{Log}|f|$) decreases showing a slope of -1 (Fig. 9). It refers to a capacitive behavior of MP in SBF during the EIS measurement [42, 43]. It may also be indicative of high corrosion resistance and large capacitive behavior of the outer surface layer [42, 44]. As shown in Fig. 9, there is a wide phase angle

peak at frequencies from 1000 Hz to 0.1 Hz with less phase angle fluctuation. In addition, the bode phase plots display an inflection in the a low frequency region below 0.1 Hz, suggesting that there are interactions of at least two time constants for the MP sample during EIS [40, 42]. It indicates that a double layer structure in the surface passive film on the MP sample [31, 33-36, 39, 42, 43]. Good fittings are also achieved between our experimental results and model by using $R_S(Qo(Ro(CtRt)))$ (Fig. 9).

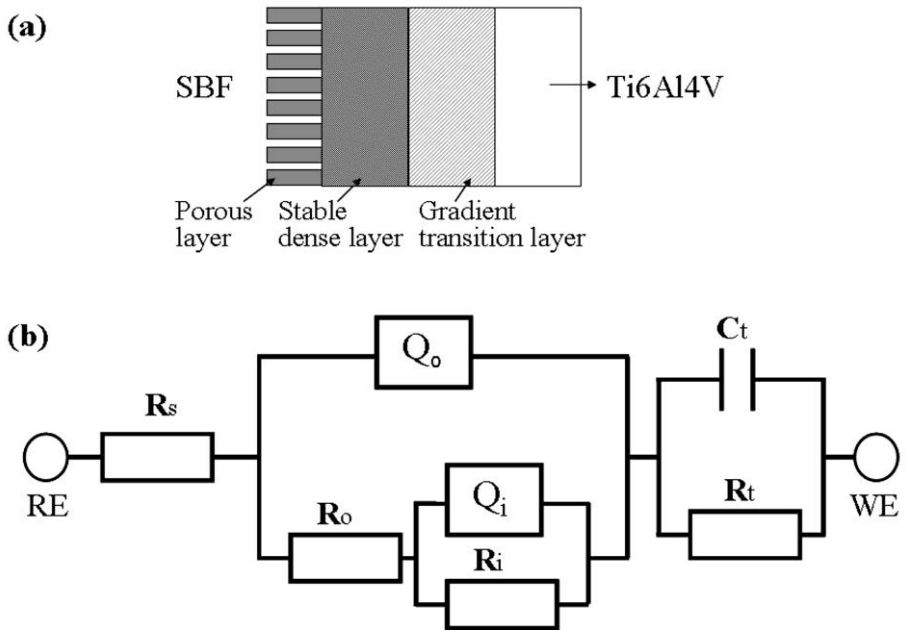

Figure 10. (a) Physical model of the interface between SBF and O-PIII Ti6Al4V alloys at open circuit potentials and (b) Equivalent electrical circuit 2 (EEC2).

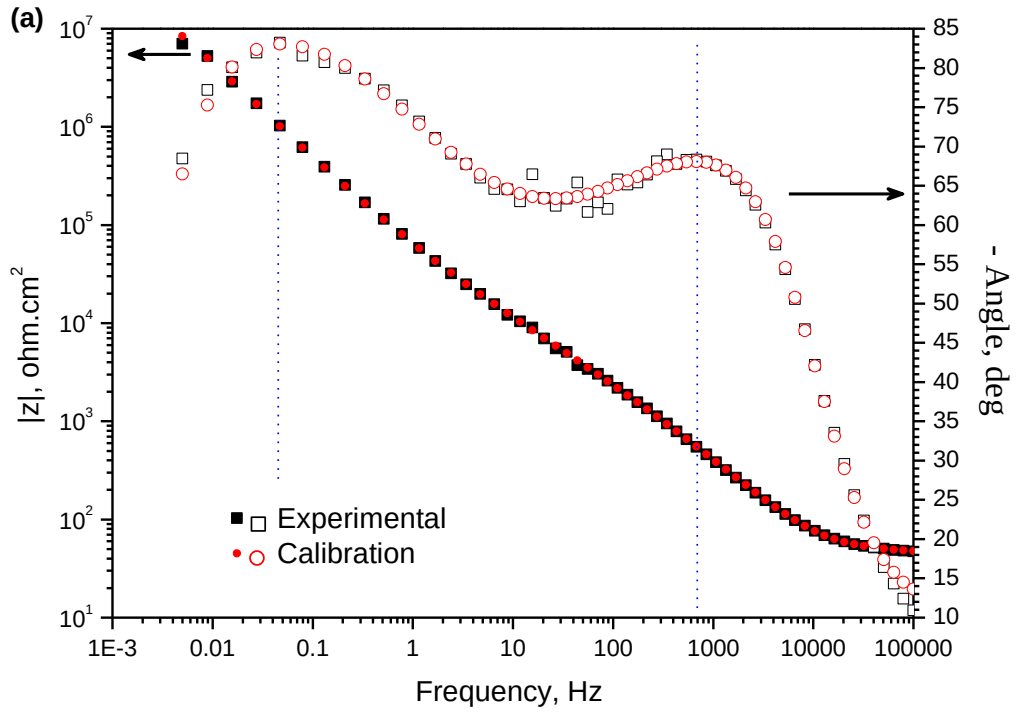

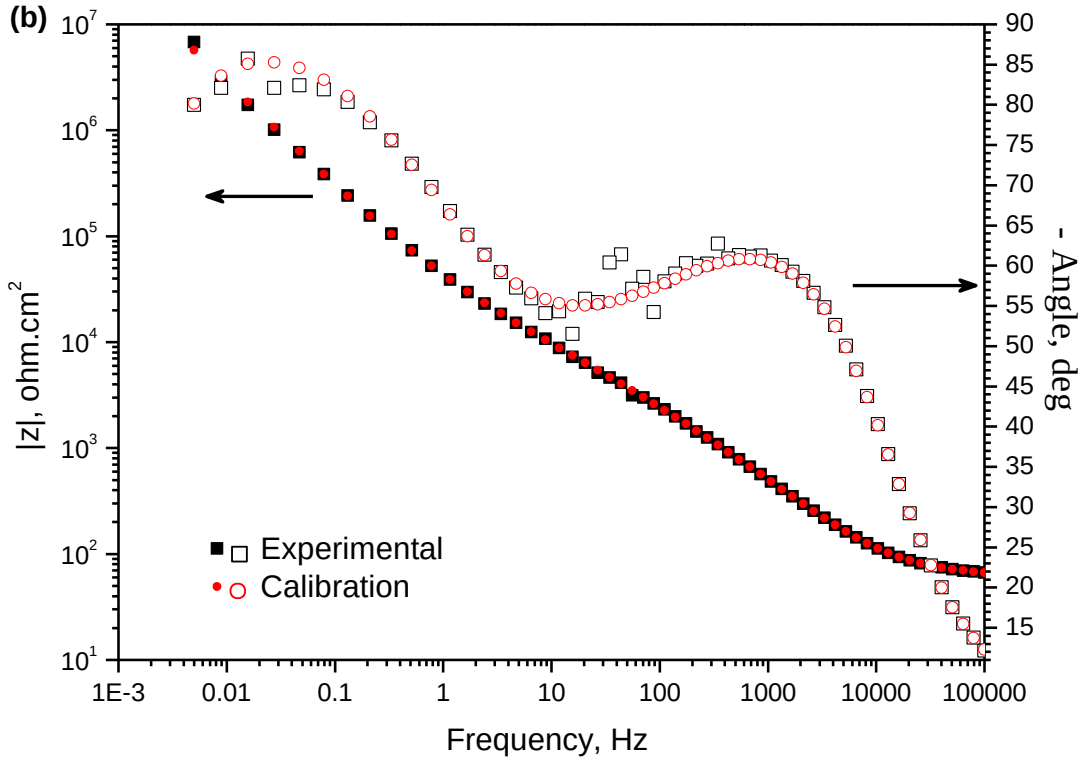
(b)
|z|, ohm.cm^2
- Angle, deg
Frequency, Hz
Experimental
Calibration
1E-3
0.01
0.1
1
10
100
1000
10000
100000

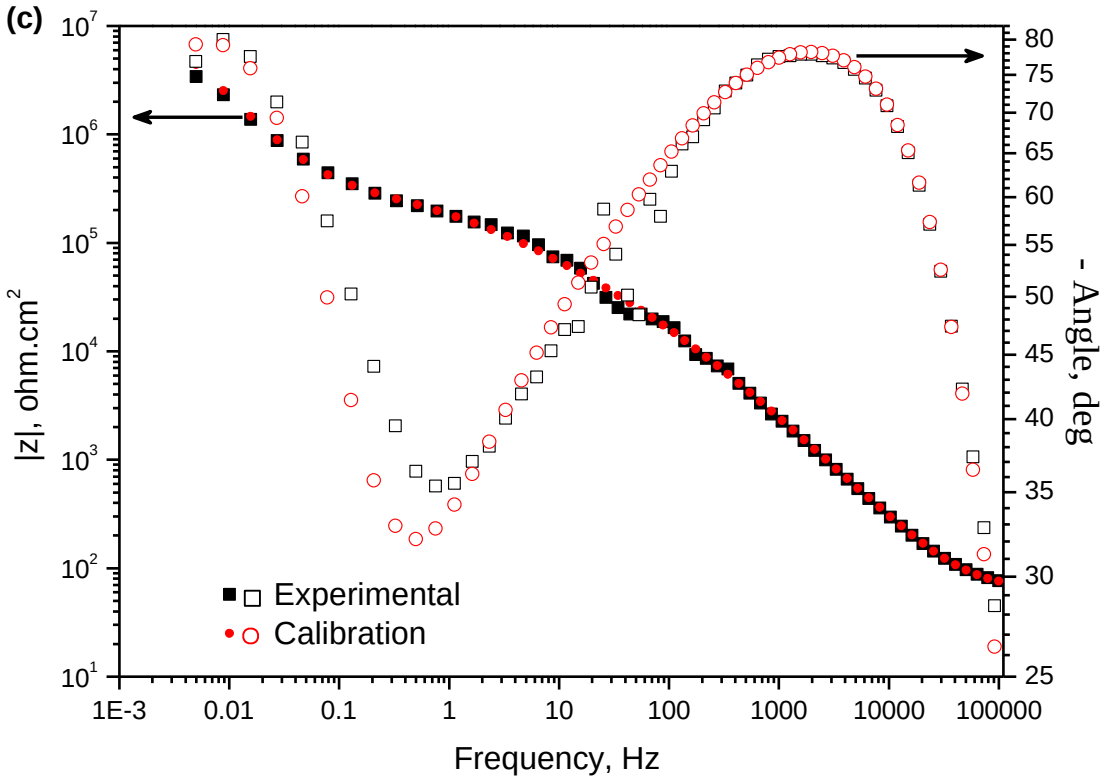
(c)
|z|, ohm.cm^2
- Angle, deg
Frequency, Hz
Experimental
Calibration
1E-3
0.01
0.1
1
10
100
1000
10000
100000

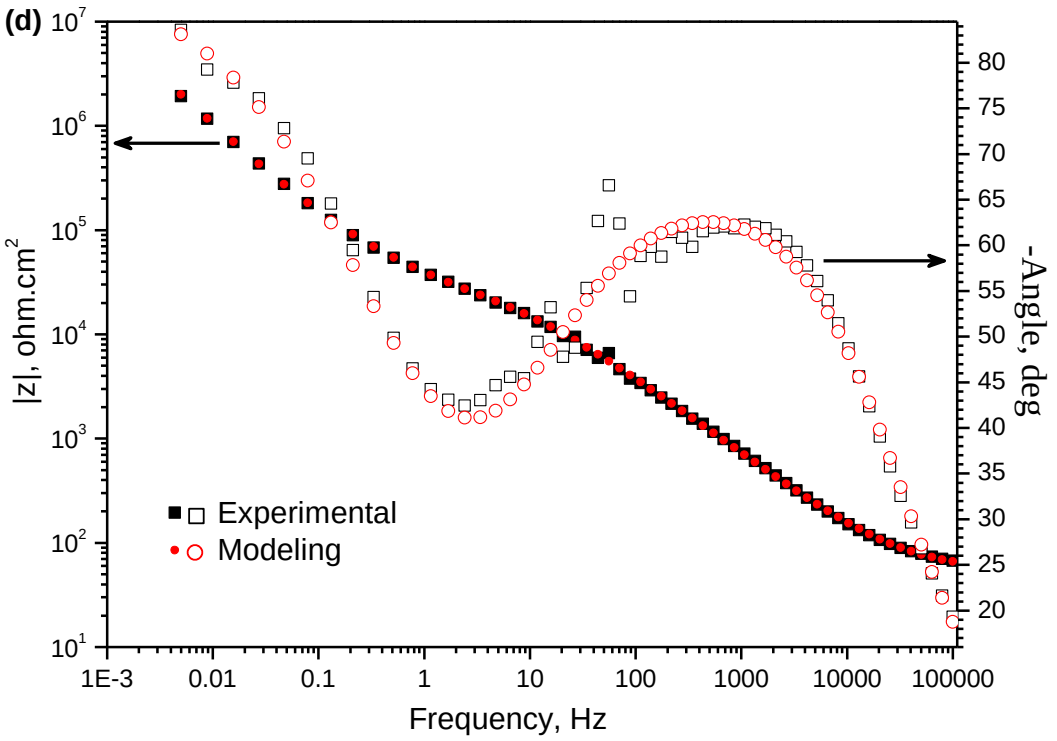

Figure 11. Bode diagrams of measured impedance spectra acquired from O-PIII TI6Al4V samples in SBF at 37 ^{o}C depending on the implantation frequency and EIS is modeled by EC2: (a) 50 Hz, (b) 200 Hz, (c) 800 Hz and (d) 400 Hz for 4 h.

According to the XPS depth profile analysis, a three-layer physical model is proposed for O-PIII treated titanium alloys and illustrated by Fig.10a. The obvious difference from the model of the MP sample is that O-PIII produces one thick and dense titanium dioxide layer followed by a bulky and gradient transition layer on the titanium substrate. The EEC2 of $R_S(Qo(Ro(QiRi)))(CtRt)$ related to this structure is proposed to model the experimental results using the software ZSimpWin. As shown in Fig. 10b, in EEC2, *Qi* and *Ri* stand for CPE and resistance of the inner dense TiO_2 layer [40-42], respectively. The other elements are the same as those in EEC1. Fig. 11 shows the experimental and modeled EIS spectra obtained from the O-PIII titanium alloys at different implantation frequencies. The EIS spectra acquired from the 50 Hz sample exhibit two obvious phase angle peaks in the bode diagram (Fig.11a). The phase angles in the high frequency and low frequency regions approach -70^{o} and -85^{o}, respectively. Furthermore, it is different from the spectra in Fig. 9 revealing that the passive film on the O-PIII titanium alloys has a different structure than that on the MP sample. The deduction is in good agreement with the XPS results. In comparison with the 50 Hz samples, the spectra obtained from the 200 Hz sample show similar two phase angle peaks in the bode diagram (Fig.11b), but the phase angle at the lowest frequency shifts from -68^{o} to about -80^{o}. As the implantation frequency is increased, the phase angle peak in the bode phase diagram shifts to the higher frequency region and covers a wider frequency range (Figs. 11b, 11c and 11d), indicating different microstructure in the passive films on these alloys [45]. Table 1 summarizes the modeled results of components in EEC2 for the evaluation of the microstructure of surface films.

Table 1. Simulation results of EIS spectra obtained from Ti6Al4V samples.

Sample	R_S (Ω cm^2)	Q_o $s^n/(\Omega cm^2)$	n1	Ro (Ω cm^2)	Qi $s^n/(\Omega cm^2)$	n2	Ri (MΩ cm^2)	Ct (μF/ cm^2)	*Rt* (MΩ cm^2)
MP	27.15	2.89×10^{-6}	0.67	27.82				0.45	5.66
50Hz	17.35	1.48×10^{-5}	0.47	37.18	2.07×10^{-5}	0.92	2.32	3.65	21.25
200Hz	61.32	1.82×10^{-6}	0.80	1445	1.93×10^{-5}	0.39	0.13	5.55	35.54
800Hz	64.46	1.10×10^{-7}	0.94	16590	1.29×10^{-6}	0.52	0.32	7.26	37.49
400Hz (4hrs)	54.13	2.01×10^{-6}	0.75	15.78	1.83×10^{-5}	0.36	21.64	18.07	14.39

Generally, the capacitance of the flat, parallel-plates capacitor is defined by the equation: $C = \varepsilon_0 \cdot \varepsilon \cdot S / d$, where ε_0 is the permittivity of free space (8.854 x 10^{-12} F/m), ε is the relative permittivity of the dielectric materials between the plates, S is the surface area of the electrode, and d is the thickness of the medium. Therefore, the thickness of the passive film can be calculated by $d = \varepsilon_0 \cdot \varepsilon \cdot S / C$. A CPE is practically associated with a pseudocapacitance. As shown in Table 1, the values of CPE (Q_o) of the O-PIII samples show the trend, i.e. $Q_o(50Hz) > Q_o(200Hz) > Q_o(800Hz)$. Therefore, the relationship of the films thickness is: $d_o(50Hz) < d_o(200Hz) < d_o(800Hz)$, which is in consistent with XPS results (Figs. 4b, 5b and 6b). However, the EIS deduction of the film thickness for the MP and 400 Hz (4 h) samples is opposite to the results by XPS depth profile. The difference may stem from surface conditions like roughness and discontinuity of the passive film. On the MP sample, natural oxidation usually induces the formation of a discontinuous passive film with a thickness of about 10 nm and the subsequent transition layer may be locally exposed to SBF. On the 400 Hz – 4 h sample, the long implantation time produces different surface structure, roughness, continuity, and compactness compared to film the other O-PIII sample (2 h). The capacitance changes significantly when the passive film has different roughness as well as chemical compositions [35]. Actually, the passive film on the titanium alloys is composed of inhomogeneous dielectric materials [35]. Similarly, the values of CPE (Q_i) have the following relationship, i.e. $Q_i(50Hz) > Q_i(200Hz) > Q_i(800Hz)$ (Table 1), indicating the relevance of the inner film thickness: $d_i(50Hz) < d_i(200Hz) < d_i(800Hz)$, as consistent with the XPS results, but the Q_i value of the 400 Hz – 4 h sample is also unexpected due to the aforementioned reason. As shown in Table 1, the C_t values of the transition layers are within the same order for the 50 Hz, 200Hz and 800 Hz samples, suggesting that they almost have the same thickness. According to the relationship between the resistance (R) and specific resistivity (ρ) of materials: $\rho = R \cdot S / d$, the variation in the resistance value, i.e. *Ro*, *Ri* and *Rt*, also indicates that each layer in the passive films formed on these samples possibly have different structures, chemical compositions, and distributions. For example, according to the XPS depth profile, there is no obvious difference in the thickness (d) of the transition layer among the O-PIII samples, but the resistance (*Rt*) fluctuates significantly (Table 1), indicating variance in the structure or chemical composition in the transition layers that determines the specific resistivity (ρ).

4. CONCLUSION

Passive films are fabricated on Ti-6Al-4V by oxygen plasma immersion ion implantation (O-PIII) and the surface properties such as surface color and corrosion resistance are studied systematically. Various colors can be produced by adjusting the parameters during O-PIII. UV-visible spectrophotometry reveals that the strongest reflection peak from the passive films shifts to a long wavelength with increasing implantation frequencies as well as time. XPS reveals that the passive films possess a tri-layered structure including a rough outer titanium dioxide film, stable intermediate titanium dioxide layer, gradient transition layer. Both EIS spectra and simulated results reveal that implantation parameters such as frequency and time significantly influence the structure and variation of the chemical composition of the passive films, which in turn determine the light reflection and interference in the passive layers and visual appearance.

ACKNOWLEDGEMENTS
This work is jointly supported by City University of Hong Kong Applied Research Grant (ARG) No. 9667038, National Natural Science Foundation of China No. 51101053, 50901032, Ministry of Education Specialized Research Foundation for Doctoral Program of Universities No. 20094208120003, and Wuhan ChenGuang Research Program Grant no. 201150431134.

References

1. H. Y. Zheng, H. X.Qian, W. Zhou, *Appl. Surf. Sci.*, 254 (2008) 2174-2178.
2. R.S. Mane, O.S. Joo, W.J. Lee, S.H. Han, *Micron*, 38 (2007) 85-90.
3. G. Jerkiewicz, B. Zhao, S. Hrapovic, B.L. Luan, *Chem. Mat.*, 20 (2008) 1877-1880.
4. M. Torrell, L. Cunha, M.R. Kabir, A. Cavaleiro, M.I. Vasilevskiy, F. Vaz, *Mater. Lett.*, 64 (2010) 2624-2626.
5. O. Van Overschelde, G. Guisbiers, M. Wautelet, *J. Phys. Chem. C*, 113 (2009) 15343–15345.
6. S. Hrapovic, B.L. Luan, M. D'Amours , G. Vatankhah, G. Jerkiewicz, *Langmuir*, 17 (2001)3051-3060.
7. J. Probst, U. Gburec, R. Thull, *Surf. Coat. Technol.*, 148 (2001) 226-233.
8. X. Zhu, J. Chen, L. Scheideler, R. Reichl, J. Geis–Gerstorfer, *Biomaterials*, 25 (2004) 4087-4103.
9. A. Biswas, P. V. S. Srikant, I. Manna, U. K. Chatterjee, J. Dutta Majumdar, *Surf. Eng.*, 24 (2008) 442-446.
10. H. Cimenoglu, M. Gunyuz, G.T. Kose , M. Baydogan , F. Ugurlu , C. Sener, *Mater. Charact.*, 62 (2011) 304-311.
11. X.M. Liu, S.L. Wu, Y.L. Chan, P.K. Chu, C.Y. Chung, C.L. Chu, K. W. K. Yeung, W. W. Lu, K. M. C. Cheung, K. D. K. Luk, *Mater. Sci. Eng. A*, 444 (2007) 192-197.
12. X.Y. Liu, P.K. Chu, C.X. Ding, *Mater. Sci. Eng. R-Rep.*, 47 (2004) 49-121.
13. S.L. Wu, X.M. Liu, T. Hu, P. K. Chu, J. P. Y. Ho, Y. L. Chan, K. W. K. Yeung, C. L. Chu, T. F. Hung, K. F. Huo, C. Y. Chung, W. W. Lu, K. M. C. Cheung, K. D. K. Luk, *Nano Lett.*, 8 (2008) 3803-3808.
14. N.F. Fahim, M.F. Morks, T. Sekino, *Electrochim. Acta*, 54 (2009) 3255-3269.
15. X.Y. Liu, P.K. Chu, C.X. Ding, *Mater. Sci. Eng. R-Rep.*, 70 (2010) 275-302.
16. J. Pan, D. Thierry, C. Leygraf, *J. Biomed. Mater. Res.*, 30 (1996) 393-402.
17. P.K. Chu, Surf. Coat. Technol. (2012), doi:10.1016/j.surfcoat.2012.03.073.
18. P.K. Chu, *IEEE Trans. Plasma Sci.*, 35 (2007) 181-187.

19. G.S. Wu, K. Feng, A. Shanaghi, Y. Zhao, R.Z. Xu, G.Y. Yuan, P. K. Chu, *Surf. Coat. Technol.*, 206 (2012) 3186-3195.
20. X.B. Tian , C.Z. Gong , S.Q. Yang , Z.J. Luo, R.K.Y. Fu, P.K. Chu, *IEEE Trans. Plasma Sci.*, 34 (2006) 1235-1240.
21. S.L. Wu, X.M. Liu, T. Hu, J. Jiang, P.K. Chu, K.W.K. Yeung, C.Y. Chung, C. L. Chu, Xu, Z.S. Xu, W. W. Lu, K.M.C. Cheung, K.D.K. Luk, *J. Electrochem. Soc.*, 156 (2009) C187-194.
22. P.K. Chu, B.Y. Tang, L.P. Wang, X.F. Wang, S.Y. Wang, N. Huang, *Rev. Sci. Instrum.*, 72 (2001) 1660-1665.
23. K. W. K. Yeung, R. Y. L. Chan, K. O. Lam, S. L. Wu, X. M. Liu, C. Y. Chung, P.K. Chu, W. W. Lu, D. Chan, K. D. K. Luk, K. M. C. Cheung, *Surf. Coat. Technol.*, 202 (2007) 1247-1251.
24. T. Kokubo, H. Kushitani, S. Sakka, T. Kitsugi, T. Yamamuro, *J. Biomed. Mater. Res.*, 24 (1990) 721-734.
25. R.J.D. Tilley, Colour and the Optical Properties of Materials: an exploration of the relationship between light, the optical properties of materials and colour, John Wiley & Sons, ISBN 0471851973, New York, (2000)
26. S. Van Gils, P. Mast, E. Stijns, H. Terryn, *Surf. Coat. Technol.*, 185 (2004) 303-310.
27. J.F. Moulder, W.F. Stickle, P.E. Sobol, K.D. Bomben, J. Chastain, Handbook of X-ray Photoelectron Spectroscopy: A Reference Book of Standard Spectra for Identification and Interpretation of XPS Data. Physical Electronics Division, Perkin- Elmer Corp, ISBN 0962702625, Minnesota, (1992)
28. Y.W. Gu, B.Y. Tay, C.S. Lim, M.S. Yong, *Appl. Surf. Sci.*, 252 (2005) 2038-2049.
29. S.L. Wu, P. K. Chu, X.M. Liu, C.Y. Chung, J.P.Y. Ho, C.L. Chu, S.C. Tjong, K.W.K. Yeung, W.W. Lu, K.M.C. Cheung, K.D.K. Luk, *J. Biomed. Mater. Res. Part A*, 79 (2006) 139-146.
30. L. Tan, W.C. Crone, *Acta Mater.*, 50 (2002) 4449-4460.
31. J. Pan, D. Thierry, C. Leygraf, *Electrochim. Acta*, 41 (1996) 1143-1153.
32. A.M. Fekry, R.M. El-Sherief, *Electrochim. Acta*, 54 (2009) 7280-7285.
33. A.M. Fekry, M.A. Ameer. *Int. J. Electrochem. Sci.*, 6 (2011) 1342-1354.
34. I.C. Lavos-Valereto, S. Wolynec, I. Ramires, A.C.Guastaldi, I. Costa, *J. Mater. Sci.-Mater. Med.*, 15 (2004) 55-59.
35. I. Milošev, T. Kosec, H.H. Strehblow, *Electrochim. Acta*, 53 (2008) 3547-3558.
36. X. M. Liu, S. L. Wu, P. K. Chu, C. Y. Chung, C. L. Chu, K. W. K. Yeung, W. W. Lu, K. M. C. Cheung, K. D. K. Luk, *Appl. Surf. Sci.*, 253(2007) 3154-3159.
37. N. A.Al-Mobarak, A. A. Al-Swayih, F. A. Al-Rashoud, *Int. J. Electrochem. Sci.*, 6 (2011) 2031-2042.
38. F. Mohammadi, T. Nickchi, M.M. Attar, A. Alfantazi, *Electrochim. Acta*, 56 (2011) 8727-8733.
39. N. Figueira, T.M. Silva, M.J. Carmezim, J.C.S. Fernandes. *Electrochim. Acta*, 54 (2009) 921-926.
40. S.L.d. Assis, S. Wolynec, I. Cost, *Electrochim. Acta*, 51 (2006) 1815-1819.
41. S. Tamilselvi, V. Raman, N. Rajendran, *Electrochim. Acta*, 52 (2006) 839-846.
42. R. Ummethala, F. Despang, M. Gelinsky, B. Basu, *Electrochim. Acta*, 56 (2011) 3809-3820.
43. R.Q. Hang, S.L. Ma, V. Ji, P.K. Chu, *Electrochim. Acta*, 55 (2010) 5551-5560.
44. J.E.G. Gonzalez, J.C. Mirza-Rosca, *J. Electroanal. Chem.* 471 (1999) 109-115.
45. S.L. Mu, N. Li, D.Y. Li, Z.L. Zou. *Electrochim. Acta*, 54 (2009) 6718–6724